Pergamon

Acta mater. Vol. 46, No. 2, pp. 609–616, 1998

Printed in Great Britain
PII: S1359-6454(97)00248-6
1359-6454/98 $19.00 + 0.00

ON THE QUANTIFICATION OF BRIDGING TRACTIONS DURING SUBCRITICAL CRACK GROWTH UNDER MONOTONIC AND CYCLIC FATIGUE LOADING IN A GRAIN-BRIDGING SILICON CARBIDE CERAMIC†

C. J. GILBERT and R. O. RITCHIE

Materials Sciences Division, Lawrence Berkeley National Laboratory and Department of Materials Science and Mineral Engineering, University of California, Berkeley, CA 94720-1760, U.S.A.

(Received 16 September 1996; accepted 1 July 1997)

Abstract—The mechanisms of cyclic fatigue-crack propagation in a grain-bridging ceramic, namely an *in situ* toughened, monolithic silicon carbide, is examined. The primary goal is to directly quantify the bridging stresses as a function of cyclic loading. To investigate the effect of the number of loading cycles on the strength of the wake bridging zone, crack-opening profiles of cracks grown at high velocity near the K_c instability (to simulate behavior on the R-curve) and at low velocity near the fatigue threshold (to simulate the cyclically-loaded crack) were measured *in situ* in the scanning electron microscope at a fixed applied stress intensity. Differences between the measured profiles and those computed for elastic traction-free cracks permit the estimation of the traction distributions. These are then used to simulate resistance curve and fatigue-crack growth rate date. Predictions are found to be in close agreement with experimental measurements on disc-shaped compact-tension specimens. The results provide direct, quantitative evidence that bridging tractions are indeed progressively diminished due to cyclic loading during fatigue-crack propagation in a grain-bridging ceramic. © *1998 Acta Metallurgica Inc.*

1. INTRODUCTION

It is now well known that the principal source of toughening during resistance-curve (R-curve) behavior in non-transforming monolithic ceramics derives from crack-wake phenomena, in particular from a zone of bridging grains behind the crack tip which screen it from the applied loads (crack-tip shielding) [1–5]. Specifically, where fracture is intergranular, the elastic and frictional tractions generated via the contact of opposing crack faces act to reduce the local driving force in the immediate vicinity of the crack tip. Indeed, various attempts have been made to quantify the magnitude and distribution of bridging tractions acting across the faces of cracks growing under monotonic loads in order to understand the mechanics of R-curve toughening and how it relates to local microstructure. For example, sawcut techniques have been employed in which the specimen compliance is monitored as the crack-wake bridging zone is sequentially eliminated with a sharp diamond saw [6, 7]; this permits not only the magnitude of bridging tractions to be determined, but also their distribution. Another approach involves slicing individual sections out of the crack wake and using these "post fracture tensile specimens" for subsequent tensile testing [8, 9]. Although both techniques yield useful information on the extent of bridging, they are clearly destructive to the specimen.

Corresponding non-destructive techniques have also been employed to determine bridging distrubutions. One method, for example, uses regression analyses to fit traction distribution functions characteristic of frictional grain pullout to the measured R-curve [4, 10–12]. Another non-destructive approach involves the measurement of crack opening profiles under an applied load, which are then compared to elastic solutions for traction-free cracks. When bridging tractions exist, the measured openings are significantly smaller than predicted (Fig. 1), and this discrepancy can then be used to calculate the traction stresses. This technique, for example, has been employed for monotonically loaded cracks in monolithic [13–15] and reinforced [16, 17] aluminas.

Under repetitive loading, it is now known that cyclic fatigue crack advance in most grain-bridging ceramics is motivated by a cycle-dependent suppression of such bridging [18–23], generally involving frictional wear processes along active bridging sites. Although a complete mechanistic understanding of cyclic fatigue at ambient temperatures is still lacking, it is clear that such degradation is fundamentally distinct from the mechanisms associated with metal fatigue. Whereas in metallic systems cyclic

†Work supported by the Director, Office of Energy Research, Office of Basic Energy Sciences, Materials Sciences Division of the U.S. Department of Energy under Contract No. DE-AC03-76SF00098.

fatigue mechanisms are associated with *intrinsic* damage *ahead* of the crack tip, the basis for cyclic fatigue-crack growth in ceramics is considered to be *extrinsic* damage *behind* the crack tip via cycle dependent, progressive suppression of crack-tip shielding. The mechanism of crack advance at or ahead of the tip is assumed to be largely unchanged from that under static loading. For example, recent modeling [18, 21] has shown that in ceramics toughened by grain-bridging mechanisms, such as hot-pressed Si_3N_4 and Al_2O_3, repetitive sliding wear of the frictional grain bridges under cyclic loading can result in reduced frictional pullout stresses, which markedly reduces the toughening capacity and locally enhances crack-tip driving forces under cyclic loads. Similar mechanisms have been analyzed for composite microstructures which derive their toughness from frictional bridging by partially bonded whiskers or fibers [24].

Accordingly, the principal goal of the present study is to quantify directly the magnitude and distribution of bridging tractions during subcritical crack growth under both static and in particular cyclic loads in a well characterized grain-bridging ceramic, specifically a high-toughness silicon carbide [25, 26], employing the crack-opening profile technique described above. *In situ* measurements for near-static loading are used to predict the R-curve, and corresponding measurements for cyclic loads are used to quantify the decay in bridging during fatigue-crack growth. Such results in turn are used to simulate fatigue crack-growth rate data.

2. EXPERIMENTAL PROCEDURES

2.1. Materials

Studies were performed on an *in situ* toughened silicon carbide, termed ABC-SiC. The ceramic was prepared by hot pressing submicron β-SiC powder, mixed with 3 wt% Al, 0.6 wt% B, and 4 wt% Apiezon wax (converted to ~2 wt% C upon pyrolysis), at 1900°C for 1 h at 50 MPa under flowing argon, as described elsewhere [25]. The resulting microstructure consists of a three-dimensional interlocking network of highly elongated and plate-like primarily α-phase (4H) grains, typically $5.5 \pm 2.4\ \mu$m long by $0.7 \pm 0.2\ \mu$m wide surrounded by ~1 nm thick amorphous Al-containing grain-boundary phase. This microstructure has excellent ambient-temperature strength (four-point bend strength of 650 ± 40 MPa) and toughness properties. The toughness results from extensive crack bridging by the plate-like grains to yield an R-curve rising from a (long-crack) initiation toughness of $K_0 \sim 5.5$ MPa$\sqrt{\text{m}}$ to a steady-state value of $K_c \sim 9.1$ MPa$\sqrt{\text{m}}$ after ~600 μm of stable crack extension [26]. Further details on the microstructure and properties of ABC-SiC are given elsewhere [25, 26].

2.2. Profile measurements

Cyclic-fatigue cracks were grown in the ABC-SiC in a room air environment at 25°C using disc-shaped compact tension DC(T) specimens (with thickness $B = 3.30$ mm, and width $W = 28.6$ mm and an initial notch length of $0.3W$). To maintain a constant crack-growth rate, da/dN, cracks were grown on a computer-controlled servo-hydraulic testing machine under stress-intensity, K, control at a frequency of 25 Hz (sine wave) with a load ratio (ratio of minimum to maximum stress intensities, $R = K_{min}/K_{max}$) of 0.1. Procedures generally met with those outlined in the ASTM fatigue-crack growth standard E647.

Two conditions were chosen to distinguish the relative effects of cyclic loading on the magnitude of bridging tractions:

- Case I: da/dN was maintained at a near-instability value of $\sim 2 \times 10^{-8}$ m/cycle, with $K_{max} = 8.4$ MPa$\sqrt{\text{m}}$, i.e. at ~92% K_c, to simulate behavior on the R-curve.†
- *Case II:* da/dN was maintained at a near-threshold value of $\sim 1 \times 10^{-10}$ m/cycle, with $K_{max} = 6.8$ MPa$\sqrt{\text{m}}$, i.e. at ~75% K_c, to simulate the cyclically-loaded crack.

In each case, the fatigue cracks were grown at least 2 mm at the rates given above prior to date collection,‡ final crack lengths (when the opening profile was measured) were 21.1 mm for Case I and 18.1 mm for Case II. The bridging zone in Case II, were the crack was grown at near-threshold levels, experienced many orders of magnitude more loading cycles. Therefore, the intent of the comparison was to discern whether the bridging tractions in Case II would be degraded relative to Case I, as one would expect from the notion of fatigue-crack advance being motivated by a cycle-dependent suppression of shielding.

Following pre-cracking, the specimens were loaded to an applied stress intensity of $K_A = 6.22$ MPa$\sqrt{\text{m}}$ on an *in situ* loading stage inside the chamber of a scanning electron microscope (SEM). Crack-opening profiles were then measured over evenly spaced distances behind the crack tip; typically this spacing was between ~15 and 20 μm. The opening at each location was measured to a resolution of better than ~20 nm. A total of approximately 100 data points were taken for each case, spanning a region of crack wake of ~1.5 mm in length. In view of the highly tortuous nature of the crack path and the large amount of scatter, the number of data points was kept large in an effort to

†• Several attempts were made to grow a crack in the ABC-SiC under purely static loading; however, the specimen failed catastrophically each time.

‡At 2×10^{-8} m/cycle (Case I) it took roughly 1 h to grow 2 mm, whereas at 1×10^{-10} m/cycle (Case II) it took just over 9 days.

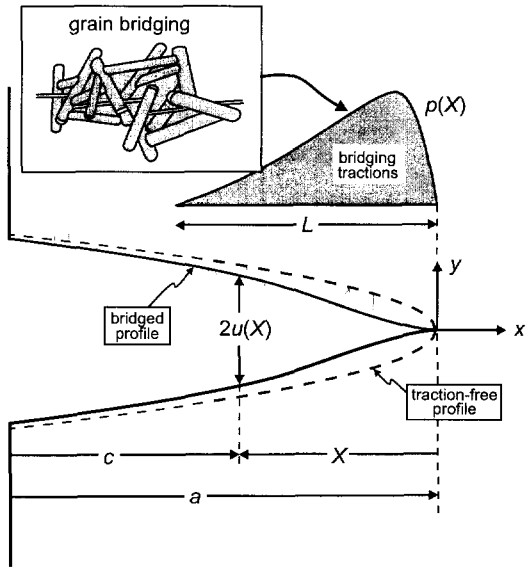

Fig. 1. Schematic of the crack-opening profile for a traction-free crack as given by equation (1) (dashed line), and a bridged crack as given by Barenblatt's solution in equation (2)(solid line). Total opening is given by $2u$, distance behind the crack tip by X, crack length by a, and $c = a - X$. The bridging zone traction distribution is denoted by $p(X)$, which acts over the bridging zone length, L, and a schematic of grain bridging is shown in the inset.

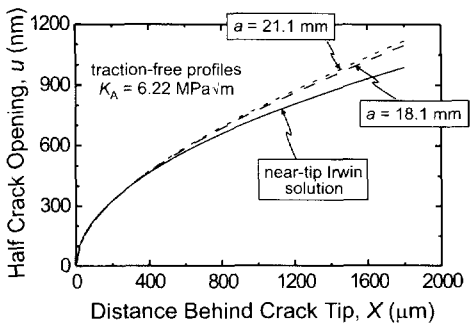

Fig. 2. Calculated crack-opening profiles for a traction-free crack under an applied stress intensity of $K_A = 6.22$ MPa$\sqrt{\text{m}}$. The solid line represents the near-field solution [equation (1)] and ignores specimen geometry. Dashed lines, however, account for specimen geometry and crack size [29–33]. Included in the plot are the calculations for both Case I (a = 21.1 mm) and Case II (a = 18.1 mm). Corrections for specimen geometry are small and do not exceed ~10%.

obtain a statistically relevant sampling of the crack-opening profile.

2.3. Calculation of crack-bridging parameters

Crack-opening displacement solutions for sharp cracks in linear elastic solids indicate that a *traction free* crack under tensile loading has a parabolic opening profile (dashed line in Fig. 1) given by (valid in the near-tip regime or when the crack is small compared to the specimen size) [27]:

$$u_{TF}(X) = \frac{K_A}{E'}\left(\frac{8X}{\pi}\right)^{1/2}, \qquad (1)$$

where $2u$ is the crack-opening displacement, X is the distance behind the crack tip, K_A is the applied stress intensity, and E' is the elastic modulus (E in plane stress or $E/(1-\nu^2)$ in plane strain, where ν is Poisson's ratio).

Under the action of bridging tractions, however, the *net opening profile*, $u(X)$, for a crack under an applied far-field stress intensity, K_A, with a bridging traction distribution, $p(X)$, of length L acting across the crack faces (solid line in Fig. 1) is obtained from [28]:

$$u(X) = \frac{K_A}{E'}\left(\frac{8X}{\pi}\right)^{1/2} + \frac{2}{\pi E'}\int_0^L p(X')\ln\left|\frac{\sqrt{X'}+\sqrt{X}}{\sqrt{X'}-\sqrt{X}}\right| dX', \qquad (2)$$

where X is the point at which the displacement is evaluated and X' is the integrated variable where the stress p acts. (Note that here p is considered negative when acting to close the crack.)

Equation (2) was used to solve for the traction distribution function, $p(X)$, at a known applied stress intensity, $K_A = 6.22$ MPa$\sqrt{\text{m}}$, and experimentally determine $u(X)$.† As this inverse problem has an infinite number of solutions for $p(X)$ which satisfy equation (2) given a known opening profile and applied far-field load [11], a physically reasonable form of the $p(X)$ function was chosen *a priori* to minimize the number of fit parameters. Specifically, a softening form of the bridging-stress function was selected [34]. This form is widely used to represent bridging tractions in many grain-bridging ceramics where frictional pullout dominates [1, 2, 8–10, 26], and is expressed as:

$$p(X) = P_{max}\left(1 - \frac{X}{L}\right)^n, \qquad (3)$$

where the function $p(X)$ describes the bridging stress distribution as a function of distance behind the crack tip, X, starting from a maximum value of P_{max} at the crack tip ($X = 0$), and falling to zero at the end of the bridging zone ($X = L$). The maximum bridging stress is equivalent to the product of the residual clamping stress acting on a grain, σ_N, due to thermal expansion anisotropies and the coefficient of friction, μ, i.e. $P_{max} = \mu\sigma_N$ [2]. The shape of the decrease is determined by the exponent n. For example, $n = 0$ corresponds to a uniformly dis-

†Note that in the present study specimen geometry effects on the crack-opening profiles as described by Fett [29–33] are ignored for simplicity. This is justified by the close correspondence of the near-tip solution given by equation (1) and those which correct for specimen geometry effects (Fig. 2). Indeed, the two solutions neven differ by more than 10% within the range of measured data.

tributed stress over the entire bridging zone, whereas $n = 1$ corresponds to the case of frictional pullout where the cross-sectional geometry of the bridging grains does not change during crack opening [35].

The parameter L was set at the maximum extent of the data ($L = 1.5$ mm). The combination of n and P_{max} which minimized the error (sum of squares) between the data and the calculated profile [equation (2)] was taken as the best fit. By performing this procedure on the data from both the near-instability (Case I) and near-threshold (Case II) cracks, it was possible to compare the effects of cyclic loading on the magnitude of bridging tractions in the wake of the crack tip. For all calculations, values of $E = 400$ GPa for the elastic modulus and $\nu = 0.25$ for Poisson's ratio were taken as being representative of polycrystalline SiC [36].

The distribution function from the near-instability case (Case I) was used to determine the bridging-stress–displacement function, $p(u)$ (representing the variation in bridging tractions with crack-opening displacement) for the ABC-SiC, as it most closely represented the bridging tractions developed during monotonic loading.† $p(u)$ can be readily calculated for this case since the best-fit $u(X)$ opening profile and the $p(X)$ distribution are both known. Inverting the function $u(X)$ into $X(u)$ allows $p(u)$ to be determined as:

$$p(u) = P_{max}\left(1 - \frac{X(u)}{L}\right)^n. \quad (4)$$

The point at which $p(u) = 0$, i.e. at the end of the bridging zone, is referred to as the critical crack opening and denoted by $2u_f$.

3. RESULTS AND DISCUSSION

3.1. Bridging tractions during near-monotonic loading

The measured crack-opening profile for Case I, where the crack was grown at ~92% K_c ($K_A = 6.22$ MPa$\sqrt{m}$), is plotted in Fig. 3 as function of distance X behind the crack tip; the calculated opening profile for a traction-free crack under the same loading conditions, $u_{TF}(X)$ from equation (1), is included for comparison (solid line). It is apparent that the shape of the measured profile is closer to linear than to parabolic; moreover, its opening is significantly smaller than that expected for the traction-free crack. Also included in this plot is the best-fit crack-opening profile determine from equation (2). The scatter evident in the opening profile data results from the highly tortuous nature of the crack path; the fit, therefore, represents average behavior.

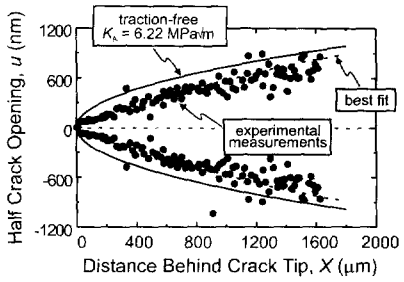

Fig. 3. The crack-opening profile for a crack grown under cyclic loading at ~92% of the fracture toughness ($da/dN \sim 2 \times 10^{-8}$ m/cycle) is plotted as a function of distance behind the crack tip, X. Included in this plot is the profile expected for a traction-free crack (solid line) at this applied stress intensity ($K_A = 6.22$ MPa$\sqrt{m}$), and the profile calculated using the best-fit bridging distribution, $p(X)$.

The fitting procedure yielded a maximum bridging stress of $P_{max} = 100$ MPa with $n = 1.4$, and the best-fit bridging distribution function, $p(X)$, is plotted in Fig. 4(a). The best-fit $p(X)$ and $u(x)$ functions were also used to calculate the $p(u)$ function [equation (4)]. This bridging stress-displacement function for the ABC-SiC is illustrated in Fig. 4(b), where the bridging stress is maximum at 100 MPa and drops to zero after a critical opening, u_f, of

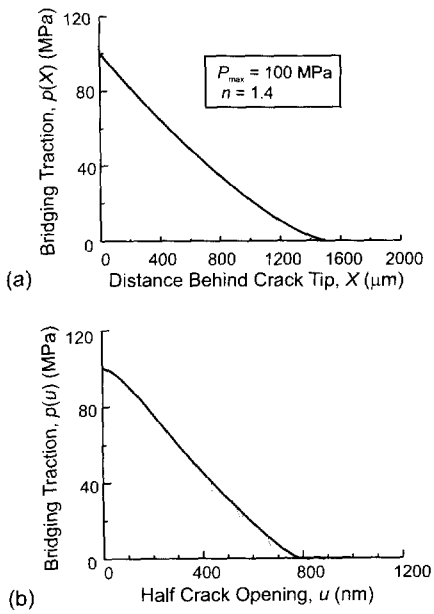

Fig. 4. The bridging stress distribution function, $p(X)$, is plotted in (a) for the crack grown at $\sim 2 \times 10^{-8}$ m/cycle (Fig. 3). The bridging stress displacement function, $p(u)$, was calculated using the best-fit crack-opening profile, $u(X)$, and the best-fit distribution function, $p(X)$, for the crack, and is plotted in (b).

†Whereas the bridging distribution function, $p(X)$, is influenced by specimen geometry and crack length, the bridging-stress–displacement function, $p(u)$, is a material property, independent of crack size and specimen geometry. Indeed the R-curves for various specimen geometries and flaw sizes can be deduced from a knowledge of $p(u)$ [29, 31] provided the appropriate weight functions are known for the specific specimen geometry (these can be found for most common geoemtries in Refs [29–33]).

790 nm ($2u_f = 1.6\ \mu m$). These values of P_{max} and n compare well with data for polycrystalline alumina, where P_{max} has been reported from 40 to 120 MPa and n and from 1 to 2.5 [5, 6, 9, 11–16]. In addition, this value of P_{max} correlates well to Raman spectroscopy measurements of internal residual stress fluctuations from grain to grain in the ABC-SiC [37]. Fluctuations as high as ~150 MPa were observed over a scale consistent with grains or small clusters of grains [37]. Such stresses, induced via thermal expansion anisotropy during cooling from processing temperatures, are known to have a large effect on bridging behavior [1, 2].

As a check on the validity of the bridging tractions determined using these fitting procedures, an R-curve was calculated from the distribution function for the near-instability case (Case I) and compared to experimentally measured behavior under monotonic loading. The bridging contribution for a crack that has propagated an amount Δa, $K_B(\Delta a)$, was determined from the bridging stress distribution, $p(X)$, via [2]:

$$K_B(\Delta a) = \left(\frac{2}{\pi}\right)^{1/2} \int_0^{\Delta a} \frac{p(X)}{\sqrt{X}} dX. \quad (5)$$

To calculate the R-curve, Δa was varied from $\Delta a = 0$ to $\Delta a = L$. With a knowledge of the long-crack initiation toughness (K_0~5.5 MPa$\sqrt{m}$ for ABC-SiC), the resistance curve, $K_R(\Delta a)$, can be determined from:

$$K_R(\Delta a) = K_0 + K_B(\Delta a). \quad (6)$$

Note this again ignores specimen geometry effects, which, as mentioned previously, are expected to be small in this case (see Fig. 2).

Using equations (5) and (6)with the best-fit $u(X)$ and $p(X)$ functions derived above, the R-curve for ABC-SiC is simulated in Fig. 5 and can be seen to be in reasonable agreement to that measured experimentally on DC(T) specimens. Indeed, the simulated R-curve is ~86% saturated after the first

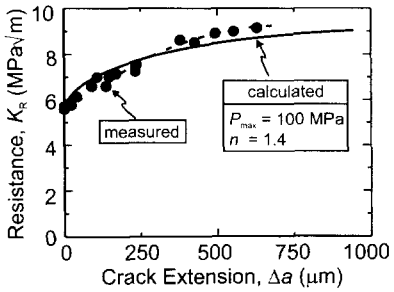

Fig. 5. A simulated R-curve (solid line) is plotted as crack-growth resistance, K_R, vs crack extension, Δa. This R-curve was calculated using the best-fit bridging distribution, $p(X)$, where the peak bridging stress, $P_{max} = 100$ MPa and the bridging exponent, $n = 1.4$. Solid circles represent the experimentally determined R-curve measured using a long-crack DC(T) specimen. The calculation was truncated at the extent of the measured data.

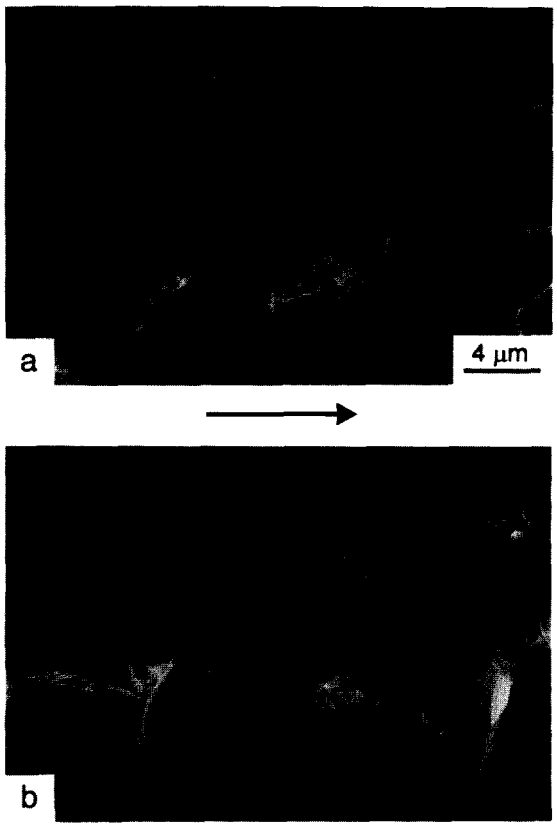

Fig. 6. SEM images of crack profiles in ABC-SiC taken after specimen failure under monotonic load; the opposing faces were carefully aligned after failure. Notice that the total pullout distance is typically on the order of several microns. Arrow indicates direction of crack growth.

600 μm of crack extension, despite the fact that L was set to 1.5 mm. Furthermore, the predicted peak toughness is 9.2 MPa$\sqrt{m}$, compared to the measured value of 9.1 MPa$\sqrt{m}$, which gives credence to the validity of this fit.

These bridging parameters are also consistent with experimentally observed bridging processes (Fig. 6). Although pullout distances varied from grain to grain, SEM observations showed that they typically ranged from ~1 to 5 μm. An alternative measure of the critical crack opening is the point where the R-curve has achieved 95% of the steady-state value (this avoids errors due to uncertainties in the value of L). Using equation (5) and the best-fit $p(X)$ distribution, 95% of the steady-state K_c value is achieved after $\Delta a \sim 880\ \mu m$. This corresponds to a critical crack opening of 520 nm (i.e. $2u_f \sim 1\ \mu m$), again consistent with SEM observations of crack profiles in Fig. 6.

3.2. *Effect of cyclic loading on bridging tractions*

The measured opening-profile (at $K_A = 6.22$ MPa$\sqrt{m}$) for the crack grown after extensive fatigue cycling at a near-threshold growth rate of $\sim 1 \times 10^{-10}$ m/cycle (Case II) is compared in Fig. 7 with the crack-opening profiles for the traction-free

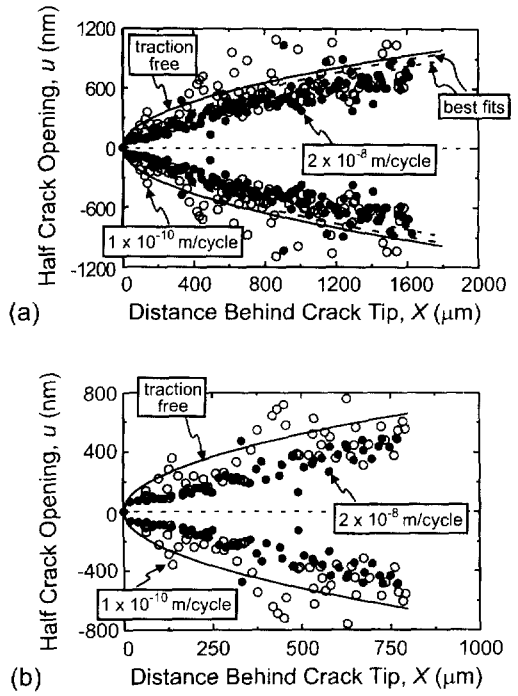

Fig. 7. The crack-opening profile for a crack grown under cyclic load near threshold ($da/dN \sim 1 \times 10^{-10}$ m/cycle) is plotted in (a) as a function of distance behind the crack tip, X. Included in this plot is the profile measured for the near-instability crack grown at $da/dN \sim 2 \times 10^{-8}$ m/cycle, as well as the traction-free profile at this applied stress intensity ($K_A = 6.22$ MPa$\sqrt{m}$). These data are replotted in (b) over the crack-tip region within which most of the steady-state toughness, K_c, is developed. The crack grown at the slower growth rate has on average a larger opening, indicative of reduced bridging tractions.

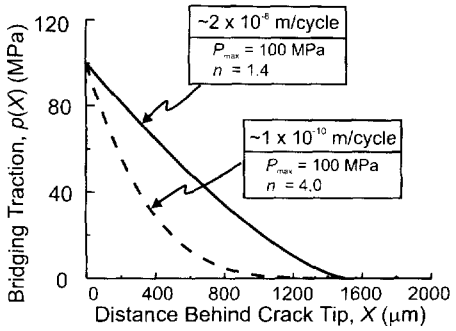

Fig. 8. Bridging traction distributions, $p(X)$, calculated for cracks grown at $\sim 2 \times 10^{-8}$ m/cycle and $\sim 1 \times 10^{-10}$ m/cycle. Notice the significant decrease in the magnitude of bridging tractions for the crack grown at a slower growth rate, attributed to more wear degradation.

crack (solid line) and for the near-instability crack, grown at $\sim 2 \times 10^{-8}$ m/cycle. It is apparent that the near-threshold crack is significantly more open than the near-instability crack and essentially straddles the profile for the traction-free crack. This is consistent with a reduction in the magnitude of bridging tractions for a bridging zone that has experienced several orders of magnitude more loading cycles. The enhanced opening is evident particularly in the near crack-tip region [Fig. 7(b)], where most of the steady-state toughness is developed (i.e. within ~ 600 μm of the tip). The best-fit $p(X)$ function from the near-threshold (Case II) crack is compared to the near-instability (Case I) crack in Fig. 8. It is clear that continued cyclic loading acts to degrade the bridging tractions; moreover, the opening profile of the crack-tip region tends toward that of a traction-free crack. This has also been observed previously in Si_3N_4 [22, 23], and is also consistent with the severe abrasion observed on fatigue fracture surfaces in the ABC-SiC [26].

The magnitude of bridging tractions measured at $da/dN \sim 1 \times 10^{-10}$ m/cycle and $da/dN \sim 2 \times 10^{-8}$ m/cycle (Fig. 8) can be used to simulate experimental cyclic fatigue-crack growth rate data. Simulation of corresponding crack-growth behavior under fatigue loading was based on the notions that the crack-advance mechanism does not change and that the influence of the cyclic loads is to progressively degrade crack bridging. This was deemed to be valid since, unlike metals or intermetallics [38], the crack-advance mechanism during fatigue-crack growth in non-transforming ceramics at ambient temperatures is identical to that occurring under monotonic loading (i.e. to static fatigue) [18–20]. The simulation procedure is summarized as follows:

- the steady-state shielding terms, K_B, for the bridging zones shown in Fig. 8 were calculated with $\Delta a = L = 1.5$ mm, using equation (5);
- the driving force, K_{max}, to maintain this growth rate, da/dN, was determined by adding this shielding term, K_B, to the long-crack initiation toughness, K_0, i.e. $K_{max} = K_0 + K_B$.

The steady-state shielding values active at a given growth rate were found to be $K_B \sim 5.5$ MPa$\sqrt{m}$ at 1×10^{-10} m/cycle and 3.7 MPa$\sqrt{m}$ at 2×10^{-8} m/cycle. Adding each of these shielding values to the long-crack initiation toughness as measured on the R-curve ($K_0 \sim 5.5$ MPa$\sqrt{m}$), the total driving force, K_{max}, required to continue fatigue-crack growth at the given velocity was determined as ~ 8.0 MPa$\sqrt{m}$ at 1×10^{-10} m/cycle and ~ 9.2 MPa$\sqrt{m}$ at 2×10^{-8} m/cycle. The predicted variation in da/dN with the stress-intensity range ($\Delta K = K_{max}/(1 - R)$) for ABC-SiC is compared in Fig. 9 with crack-growth rate data experimentally measured on DC(T) specimens at $R = 0.1$ [26]. Using a simplified form of the Paris law where $da/dN = C'(\Delta K)^m$, a regression fit of the simulated date yields values of $m = 38$, compared to the experimentally measured value of $m = 37$. A comparison of predicted and experimental fatigue results are summarized in Table 1.

The growth rates simulated from the crack-opening profile data can be seen to be in reasonably close agreement, although marginally underpredicting, the experimentally measured growth rates. The

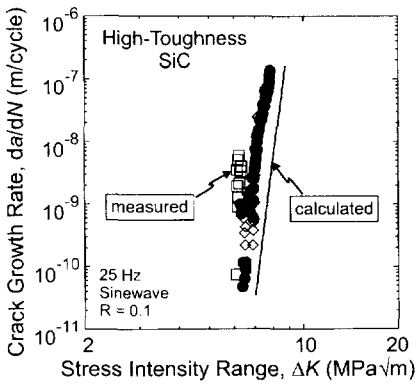

Fig. 9. Simulated fatigue crack-growth rates (solid line) are plotted as crack-growth rate, da/dN, vs the applied stress intensity range, ΔK. The fatigue data were calculated using the best-fit bridging distributions for the cracks grown near threshold (Case II) and near instability (Case I). Open and closed symbols represent experimental data from several specimens.

closeness of this fit in addition to the direct quantitative evidence of a cycle-induced degradation in shielding imply that the essential physics of the cyclic-crack growth process involves the cycle-dependent degradation of the active bridging zone.

4. SUMMARY AND CONCLUSIONS

A study has been made of the mechanisms of cyclic fatigue-crack propagation in a high-toughness, grain-bridging monolithic ceramic, ABC-SiC, specifically to examine the bridging stresses as a function of cyclic loading. In order to investigate the effect of the number of loading cycles on the strength of the bridging zone in the wake, cracks were grown in cyclic fatigue, both at a relatively high velocity near the K_c instability (to simulate behavior on the R-curve) and at a low velocity near the fatigue threshold (to simulate the cyclically-loaded crack). Using well-established elastic solutions, the bridging tractions were determined in each case by *in situ* measurement of the crack-opening profiles at a fixed applied load in the scanning electron microscope. Differences between expected profiles for traction-free cracks and the measured profiles were then utilized to estimate the traction distributions. The magnitude of the bridging stresses were shown to correlate very well to:

Table 1. Simulated vs experimental fatigue-crack growth parameters Paris fit parameters

	Experimental	Simulated
Threshold, ΔK_{TH} (MPa$\sqrt{m}$)	6.4	8.0
m	37	38
C (m/cycle) (MPa$\sqrt{m}$)$^{-m}$	6.5×10^{-41}	3.2×10^{-43}

- simulation of experimentally measured resistance-curves;
- simulation of experimentally measured fatigue-crack growth rate behavior;
- SEM observations of grain bridging and the pull-out process.

These results provide direct, quantitative evidence that bridging tractions are indeed progressively diminished due to cyclic loading during fatigue-crack propagation in a grain-bridging ceramic.

Acknowledgements—This work was supported by the Director, Office of Energy Research, Office of Basic Energy Sciences, Materials Sciences Division of the U.S. Department of Energy under Contract No. DE-AC03-76SF00098. Thanks are due to Dr J. J. Cao and Prof L. C. De Jonghe for processing the ABC-SiC material and for numerous helpful discussions, as well as Dr J. W. Ager, III, for Raman spectroscopy measurements.

REFERENCES

1. Evans, A. G., *J. Am. Ceram. Soc.*, 1990, **73**, 187.
2. Lawn, B. *Fracture of Brittle Solids*. 2nd ed. Cambridge University Press, New York, (1993).
3. Knehans, R. and Steinbrech, R. W., *J. Mater. Sci. Lett.*, 1982, **1**(8), 327.
4. Steinbrech, R. W., Reichl, A. and Schaarwächter, W., *J. Am. Ceram. Soc.*, 1990, **73**(7), 2009.
5. Swanson, P. L., Fairbanks, C. J., Lawn, B. R., Mai, Y.-W. and Hockey, B. J., *J. Am. Ceram. Soc.*, 1987, **71**(4), 279.
6. Hu, X. Z. and Wittmann, F. H., *J. Mater. Civil Eng.*, 1990, **2**(1), 15.
7. Hu, X. Z., Lutz, E. H. and Swain, M., *J. Am. Ceram. Soc.*, 1991, **74**(8), 1828.
8. Hay, J. C. and White, K. W., *Acta metall. mater.*, 1992, **40**(11), 3017.
9. Hay, J. C. and White, K. W., *J. Am. Ceram. Soc.*, 1993, **76**(7), 1849.
10. Mai, Y.-W. and Lawn, B. R., *J. Am. Cream. Soc.*, 1987, **70**(4), 289.
11. Cox, B. N. and Marshall, D. B., *Acta. metall. mater.*, 1991, **39**, 579.
12. Fett, T., Munz, D. and Thun, G., *J. Am. Ceram. Soc.*, 1995, **78**(4), 949.
13. Rödel, J., Kelly, J. and Lawn, B. R., *J. Am. Ceram. Soc.*, 1990, **73**(11), 3313.
14. Fett, T., *J. Am. Ceram. Soc.*, 1995, **78**(4), 945.
15. Sohn, K.-S., Lee, S. and Baik, S., *J. Am. Ceram. Soc.*, 1995, **78**(5), 1401.
16. Fett, T., Munz, D., Yu, C. T. and Kobayashi, A. S., *J. Am. Ceram. Soc.*, 1994, **77**, 3267.
17. Yu, C. T. and Kobayashi, A. S., *Ceram. Eng. Sci. Proc.*, 1993, **14**(78), 273.
18. Dauskardt, R. H., *Acta metall. mater.*, 1993, **41**(9), 2765.
19. Jacobs, D. S. and Chen, I.-W., *J. Am. Ceram. Soc.*, 1995, **78**(3), 513.
20. Gilbert, C. J., Dauskardt, R. H. and Ritchie, R. O., *J. Am. Ceram. Soc.*, 1995, **78**(9), 2291.
21. Lathabai, S., Rödel, J. and Lawn, B., *J. Am. Ceram. Soc.*, 1991, **74**(6), 340.
22. Kishimoto, H., Ueno, A. and Kawamoto, H. in *Cyclic Fatigue in Ceramics*. ed. H. Kishimoto, T. Hoshide, N. Okabe. Elsevier, (1995), p. 101.
23. Ramamurty, U., Hansoon, T. and Suresh, S., *J. Am. Ceram. Soc.*, 1994, **7**(11), 2985.

24. Rouby, D. and Reynaud, P., *Composites Sci. Tech.*, 1993, **48**, 109.
25. Cao, J. J., MoberlyChan, W. J., De Jonghe, L. C., Gilbert, C. J. and Ritchie, R. O., *J. Am. Ceram. Soc.*, 1996, **79**(2), 461.
26. Gilbert, C. J., Cao, J. J., MoberlyChan, W. J., De Jonghe, L. C. and Ritchie, R. O., *Acta mater.*, 1996, **44**(8), 3199.
27. Irwin, G. R., in *Hanbuch der Physik*, Vol. 6. Springer-Vaerlag, Berlin 1958, p. 551.
28. Barenblatt, G. I., *Adv. Appl. Mech.*, 1962, **7**, 55.
29. Fett, T., Mattheck, C. and Munz, D., *Eng. Fract. Mech.*, 1987, **27**(6), 697.
30. Fett, T., Munz, D., Seidel, J., Stech, M. and Rödel, J., *J. Am. Ceram. Soc.*, 1996, **79**(5), 1189.
31. Fett, T. and Munz, D. Stress intensity factors and weight functions for one-dimensional cracks. KfK-Report 5290, Kernforschungszentrum Karlsruhe, Karlsruhe, Germany, 1994.
32. Fett, T., *Int. J. Fract.*, 1988, **36**, 55.
33. Fett, T., *Int. J. Fract.*, 1993, **63**, R81.
34. Foote, R. M., Mai, Y.-W. and Cotterell, B., *J. Mech. Phys. Solids*, 1986, **34**(6), 593.
35. Evans, A. G., Heuer, A. H. and Porter D. L. in *Fracture 1977*. ed. D. M. R. Taplin, Vol. 1. University of Waterloo Press, Waterloo, p. 529. 1977.
36. Li, Z. and Bradt, R. C., in *Ceramic Transactions: Silicon Carbide '87*, edited by J. D. Cawley and C. E. Semler, Vol. 2, 313, The American Ceramic Society, Westerville, Ohio 1987.
37. Ager, III, J. W. Unpublished research. Lawrence Berkeley National Laboratory, 1997.
38. Venkateswara, Rao K. T., Gilbert, C. J. and Ritchie, R. O., in *Processing and Design Issues in High Temperature Materials*, ed. N. S. Stoloff and R. H. Jones, The Minerals, Metals and Materials Society, Warrendale, PA, p. 209, 1996.